Scientific Research Publishing

World Journal of Mechanics, 2022, 12, 1-16
https://www.scirp.org/journal/wjm
ISSN Online: 2160-0503
ISSN Print: 2160-049X

A Comparative Study for Compressible Turbulence Models

Hechmi Khlifi, Adnan Bourehla

Laboratory of Aeronautical Structure and Control of System Flows, SACES (UR17DN01), School of Military Avition, Borj el Amri, Tunisia
Email: khlifihachmi@yahoo.fr, bourehla@gmail.com

How to cite this paper: Khlifi, H. and Bourehla, A. (2022) A Comparative Study for Compressible Turbulence Models. *World Journal of Mechanics*, **12**, 1-16.
https://doi.org/10.4236/wjm.2022.121001

Received: March 12, 2021
Accepted: January 28, 2022
Published: January 31, 2022

Abstract

The incompressible models for the pressure-strain correlation are unable to correctly predict the turbulence flows evolving with significant compressibility. Huang and Fu use a damping function of the turbulent Mach number to modify two numerical coefficients of the incompressible model for the pressure strain developed by Launder, Reece and Rodi. This model predicts the spreading rate and the shear stress behavior in compressible turbulent mixing well. However, the model does not show the well-known compressibility effects on the compressible homogenous shear flow. In the present work, the model of Huang-Fu is revised, all resulting model coefficients become dependent on the turbulent Mach number, the gradient Mach number and the convective Mach number. The proposed model is tested in different compressible turbulent homogeneous shear flow and mixing layers cases. In general, the predicted results from the proposed model are in an acceptable agreement with DNS and experiment data.

Keywords

Turbulence, Compressible, Model, Pressure-Strain

1. Introduction

Many studies carried out in the last decade have shown that the compressibility has important effects on turbulence flows. One of the well-known effects is the reduction of the turbulent kinetic energy redistribution phenomenon. Extensive studies [1]-[6] have been conducted to study the compressible homogeneous shear flow. In this context, the DNS results [1] [3] [5] are selected as the basic documents to understand some physical discrepancies of the compressibility effects on homogeneous turbulent shear flows. The analysis of these DNS results suggests that

compressibility effects are related to extra-parameters: the turbulent Mach number $M_t\left(M_t=\sqrt{2K}/\bar{a}\right)$, where $\bar{a}$ is the mean speed of sound) and the gradient Mach number which is defined by: $M_g=Sl/\bar{a}$, where $S=\left(\tilde{U}_{i,j}\tilde{U}_{j,i}\right)^{0.5}$ and l are the mean shear constant and an integral length scale respectively. The DNS [1] [2] [4] [5] indicates that compressibility effects cause a notable reduction in the growth rate of the turbulent kinetic energy. So the turbulence modeling is essential for predicting compressibility effects in agreement with numerical and experimental data. According to the DNS results [1] [5], the structural compressibility effects cause reduction of the pressure field and then the reduction of the pressure strain correlation, which leads to the dramatic changes in the magnitude of the Reynolds stress anisotropy components. The experiments [7] [8] and the DNS results [9] [10] [11] reached similar conclusions concerning the role of pressure in the developed compressible plane mixing layers. As a consequence, in several studies, the pressure strain modeling has been considered as important attractive research in the second-order closure for the compressible turbulence flows. Different compressibility corrections using turbulent Mach number and gradient Mach number of the incompressible pressure strain model have been proposed by several authors [12] [13] [14] [15] [16]. At compressibility effects levels, the models have well predicted different characteristic parameters in some turbulence configurations. However, they failed in other configurations for which the compressibility is higher.

In this study, a revision of the model of Huang and Fu [12] of the pressure strain correlation is made making all coefficients depend on the turbulent Mach number, the gradient Mach number and the convective Mach number. The ability of Huang *et al.* [12] and the proposed model to predict compressible homogeneous shear and mixing layers are examined by considering different initial conditions. Comparison between the predictions models with DNS and experiments data shows that the proposed model describes better compressibility effects on the turbulence.

2. Basic Equations

Classically, The basic equations describing the motion of a compressible flow are the Navier-Stokes energy and state equations which can be written as follow for continuity, momentum and energy conservation equations [15] [16]:

$$\rho_{,t}+\left(\rho u_i\right)_{,i}=0, \tag{1}$$

$$\left(\rho u_i\right)_{,t}+\left(\rho u_i u_j\right)_{,j}=\sigma_{ij,j}, \tag{2}$$

$$\left(\rho e\right)_{,t}+\left(\rho e u_j\right)_{,j}=\left(\sigma_{ij}u_i\right)_{,j}-\left(\kappa T_{,j}\right)_{,j}, \tag{3}$$

where, $e=c_vT$, $\sigma_{ij}=-p\delta_{ij}+\tau_{ij}$ and $\tau_{ij}=2\mu\left(u_{i,j}+u_{j,i}\right)$.

These equations are coupled by the state equation:

$$p=\rho RT. \tag{4}$$

For compressible turbulent flow, it is well known that the basic equations of the mean quantities used in describing turbulence closure schemes are essentially those using the density weighting technique which is referred to as the Favre averages. Thus, the Favre averaged continuity, momentum, specific internal energy and the state equations are respectively written as follows [16]:

$$\bar{\rho}_{,t} + \left(\bar{\rho}\tilde{U}_i\right)_{,i} = 0, \tag{5}$$

$$\left(\bar{\rho}\tilde{U}_i\right)_{,t} + \left(\bar{\rho}\tilde{U}_i\tilde{U}_j\right)_{,i} = \left(\tilde{\sigma}_{ij} + \overline{\tau''_{ij}} - \overline{\rho u''_i u''_j}\right)_{,j}, \tag{6}$$

$$\left(\bar{\rho}\tilde{e}\right)_{,t} + \left(\bar{\rho}\tilde{e}\tilde{U}_j\right)_{,j} = -\phi_e + \pi_d - \left(\bar{c}_v\,\overline{\rho u''_j T''}\right)_{,j}, \tag{7}$$

$$\bar{p} = \bar{\rho}R\tilde{T}, \tag{8}$$

where $\phi_e = \bar{p}\left(\tilde{U}_i + \overline{u''_i}\right)_{,i} + \left(\overline{\kappa T}_{,i}\right)_{,i} + \overline{\tau_{ij}u_{i,j}}$, $\tilde{\tau}_{ij} = 2\bar{\mu}\tilde{S}_{ij} - (2/3)\bar{\mu}\tilde{U}_{k,k}\delta_{ij}$ and $\pi_d = \overline{p'u'_{i,i}}$.

For the compressible turbulence, the commonly Favre Reynolds stress models is used in this study to describe the Reynolds stress $R_{ij} = \overline{\rho u''_i u''_j}/\bar{\rho}$ as follow [16]:

$$\left(\bar{\rho}R_{ij}\right)_{,t} + \left(\bar{\rho}\tilde{U}_m R_{ij}\right)_{,m} = Pr_{ij} + D_{ij} + \varphi_{ij} + \varepsilon_{ij} + V_{ij}, \tag{9}$$

where the symbols Pr_{ij}, D_{ij}, φ_{ij}, ε_{ij} and V_{ij}, represent turbulent production, turbulent diffusion, pressure strain correlation, turbulent dissipation and the mass flux variation respectively.

$$Pr_{ij} = -\bar{\rho}R_{jm}\tilde{U}_{i,m} - \bar{\rho}R_{im}\tilde{U}_{j,m},$$

$$D_{ij} = -\left(\overline{\rho u''_i u''_j u''_m} + \overline{p'u''_j}\delta_{im} + \overline{p'u''_i}\delta_{jm} - \overline{\tau''_{im}u''_j} - \overline{\tau''_{jm}u''_i}\right)_{,m}$$

$$\varphi_{ij} = \overline{p'\left(u''_{i,j} + u''_{j,i}\right)} = \varphi^*_{ij} + 2/3\,\overline{p'u''_{k,k}}\delta_{ij}, \quad \varepsilon_{ij} = \overline{\tau''_{im}u''_{j,m}} - \overline{\tau''_{jm}u''_{i,m}}$$

$$V_{ij} = -\bar{p}_{,j}\overline{u''_i} - \bar{p}_{,i}\overline{u''_j} + \tilde{\tau}_{im,m}\overline{u''_j} + \tilde{\tau}_{jm,m}\overline{u''_i}.$$

Here, the isotropic model for the dissipation tensor ε_{ij}, is used [16]:

$$\varepsilon_{ij} = 2/3\,\varepsilon\delta_{ij}. \tag{10}$$

And the dissipation rate ε, is written as in [3]:

$$\varepsilon = \varepsilon_s + \varepsilon_c, \tag{11}$$

where for homogeneous shear flow turbulence $\bar{\rho}\varepsilon_s = \overline{\mu\omega'_i\omega'_i}$, ω'_i is the fluctuating vorticity, and $\varepsilon_c = 4/3\,\overline{\mu u'^2_{k,k}}$. Commonly used as in several studies, the solenoidal part of the dissipation can be described by the incompressible model [16], namely:

$$\left(\bar{\rho}\varepsilon_s\right)_{,t} + \left(\bar{\rho}\varepsilon_s\tilde{U}_k\right)_{,k} = \bar{\rho}\varepsilon_s\left(C_{\varepsilon 1}R_{km}\tilde{U}_{k,m} - C_{\varepsilon 2}\varepsilon_s\right)/K - \left(C_{\varepsilon 3}\bar{\rho}K/\varepsilon_s R_{km}\varepsilon_{s,m}\right)_{,k}. \tag{12}$$

The compressible dissipation rate ε_c, is determined by the models as [3]:

$$\varepsilon_c = \alpha M_t^2\varepsilon_s. \tag{13}$$

α is a numerical coefficient model, α; 0.5.

3. Compressible Turbulence Models for the Pressure Strain

Several DNS and experiment results have been carried out on compressible turbulent flows show the significant compressibility effects on the pressure field which in turn affect the pressure-strain correlation. Such effects cause reduction in the magnitude of the anisotropy of the Reynolds shear stress and increase in the magnitude of the normal stress anisotropy. Thus, the pressure-strain correlation requires a careful modeling in the Reynolds stress turbulence model. In this context, different compressible models have been developed for this term. Most of these models are generated from a simple extension of its incompressible counter-part [17] [18].

Launder Reece and Rodi Model [17]

Launder Reece and Rodi developed a model for the pressure-strain correlation namely:

$$\begin{aligned}\varphi_{ij}^{*} = &-C_1\bar{\rho}\varepsilon_s b_{ij} + C_2\bar{\rho}K\left(\tilde{S}_{ij} - \tilde{S}_{ll}\delta_{ij}\right) + C_3\bar{\rho}K\left[b_{ik}\tilde{S}_{jk} + b_{jk}\tilde{S}_{ik} - b_{ml}\tilde{S}_{ml}\delta_{ij}\right] \\ &+ C_4\bar{\rho}K\left[b_{ik}\tilde{\Omega}_{jk} + b_{jk}\tilde{\Omega}_{ik}\right]\end{aligned} \tag{14}$$

where $C_1 = 3$, $C_2 = 0.8$, $C_3 = 1.75$ and $C_4 = 1.34$.

Model of Huang and Fu [12]

Huang and Fu [12] use a damping function in compressible mixing layers to modify the LRR model for the pressure strain as follows:

$$\begin{aligned}\varphi_{ij}^{*} = &-C_1\bar{\rho}\varepsilon_s b_{ij} + C_2\bar{\rho}K\left(\tilde{S}_{ij} - \tilde{S}_{ll}\delta_{ij}\right) + C_3\bar{\rho}K\left[b_{ik}\tilde{S}_{jk} + b_{jk}\tilde{S}_{ik} - b_{ml}\tilde{S}_{ml}\delta_{ij}\right] \\ &+ C_4\bar{\rho}K\left[b_{ik}\tilde{\Omega}_{jk} + b_{jk}\tilde{\Omega}_{ik}\right]\end{aligned} \tag{15}$$

where $C_1 = 3.6$, $C_2 = 0.8$, $C_3 = 1.2 + 0.25\exp\left(-0.05/M_t^3\right)$ and $C_4 = 1.2 - 0.25\exp\left(-0.05/M_t^3\right)$.

A Proposed Model

The compressibility extension of the incompressible LRR [17] model developed by Huang *et al.* [12] explicitly involve the turbulent Mach number. As can be seen in Equation15, the model of Huang *et al.* [12] is based on a compressibility correction of the coefficients C_3 and C_4, which affect the polynomial linear term of the Reynolds stress and the mean strain rate, the other coefficients, C_2, which affects the mean strain rate, and C_1 of the return to isotropy model, are conserved as in the LRR model, without any compressibility correction. On the other hand, different analyses have been carried to show the influence of the pressure—strain on the Reynolds stress behavior. Hamba [2] presented a fine analysis for the compressible homogeneous shear flow case, and confirmed that the reduction of the transverse component P_{22} of the pressure—strain correlation principally caused the reduction of the transverse Reynolds stress R_{22}, which in turn induced a systematic reduction of the shear Reynolds stress, the streamwise component P_{11} of the pressure—strain, and then the growth rate of the turbulent kinetic energy. Thus, the compressibility correction of the coefficients C_3 and C_4 seem to be sufficient to capture compressibility effects. In this context, according

to Park *et al.* [14] and Huang *et al.* [12], in addition to the compressibility correction of the coefficients C_3 and C_4, the coefficient C_2 should be corrected with compressible parameters, such as M_t and M_g, or others. One can see that C_2 directly affects the shear component P_{12} of the pressure—strain, which has an evident contribution in the transport equation for the Reynolds shear stress, R_{12}. On the other hand, the reduction of P_{12}, which works as a sink term in the transport equation for R_{12}, leads to an increase in the growth rate of the turbulent kinetic energy via the growth of R_{12}. This is not suitable using model. So, more attention should be paid to the modeling for P_{12}. Khlifi *et al.* [16] considered an equation of the dilatation fluctuation to modify the incompressible C_2 and the retour to isotropy C_1-coefficients [16], as follows:

$$C_2 = 0.8\left(1+0.45M_t^4\right)\exp\left(-0.015M_g\right) \tag{16}$$

$$C_1 = 3\left(1-0.7M_t^2\right) \tag{17}$$

Equation (16) exhibits a C_2—dependence with M_t, M_g and M_t^4. It is noted that the term M_t^4 in model Khlifi *et al.* [16], came from the isotropic model of the turbulent dissipation rate $\varepsilon_s/\varepsilon_c$ to distinguish between low-M_t and high-M_t regimes. But this link seems to be not adaptable to Huang *et al.* [12] in calculation of the mixing layers. For this modeling, the model [3] for $\varepsilon_s/\varepsilon_c$ which linked to M_t^2 was chosen in this study. Thus, all of the coefficients of the Huang *et al.* [12] model are expressed as a function of M_t, M_g and M_c. Considering Equations (11) and (12), the proposal coefficients models are summarized in the next section.

4. Applications of the Models

4.1. Simulation of Compressible Homogeneous Shear Flow

For compressible homogeneous shear flow, the mean velocity gradient is given by:

$$\tilde{U}_{i,j} = S\delta_{i1}\delta_{j2}, \tag{18}$$

where, S is the mean shear rate.

The Favre averaged basic second order model equations are:

Table 1. Coefficients models of the pressure strain correlation for homogeneous shear flow.

Model	C_1	C_2	C_3	C_4
Model 1: Huang *et al.* [12]	3.6	0.8	$1.2+0.25\exp\left(-0.05/M_t^3\right)$	$1.2-0.25\exp\left(-0.05/M_t^3\right)$ $1.2+0.25\exp(-0.05/M_t^3)$ $1.2+0.25\exp(-0.05/M_t^3)$
Model 2: Proposal model	$3\left(1.0-0.8M_t^2\right)$	$0.8\left(1+0.45M_t^2\right)\mathrm{e}^{-0.015M_g}$	$1.2+0.25\exp\left(-0.05/M_t^3\right)$	$1.2-0.25\exp\left(-0.05/M_t^3\right)$

$$\overline{\rho}\left(R_{ij}\right)_{,t} = Pr_{ij} + \varphi_{ij}^{*} - 2/3\left[\overline{\rho}\left(\varepsilon_s + \varepsilon_c\right)\delta_{ij} - \overline{p'd'}\delta_{ij}\right], \tag{19}$$

$$\overline{\rho}\left(\varepsilon_s\right)_{,t} = \left(\overline{\rho}\varepsilon_s/K\right)\left[C_{\varepsilon 1}R_{km}\tilde{U}_{k,m} - C_{\varepsilon 2}\varepsilon_s/K\right]. \tag{20}$$

As we can see the above models are parameterized by turbulent Mach number, such a parameter is described by the transport equation as follow [16]:

$$\left(M_t\right)_{,t} = \left(M_t/2\overline{\rho}K\right)\left[P + \left(1 + 0.5\gamma\left(\gamma - 1\right)M_t^2\right)\left(\overline{p'd'} - \overline{\rho}\varepsilon\right)\right], \tag{21}$$

where $P = -\overline{\rho}R_{ij}\tilde{U}_{i,j}$ is the turbulent production and $\gamma = c_p/c_v$.

Models [3] are chosen for the dilatational terms:

$$\overline{p'd'} = -0.15M_t P + 0.2M_t^2\varepsilon_s, \quad \varepsilon_c = 0.5M_t^2\varepsilon_s \tag{22}$$

Results and Discussion

In this section, the fourth-order Runge-Kutta numerical scheme is used to numerically solve the averaged transport Equations (19), (20) and (21) to predict compressible homogeneous shear flow.

Figures 1-6 show comparison between the predictions obtained by the proposed models referred to model 2 and those from model 1 developed by Huang and Fu [12] and with the DNS [5] results, the detailed of the models are listed in Table 1.

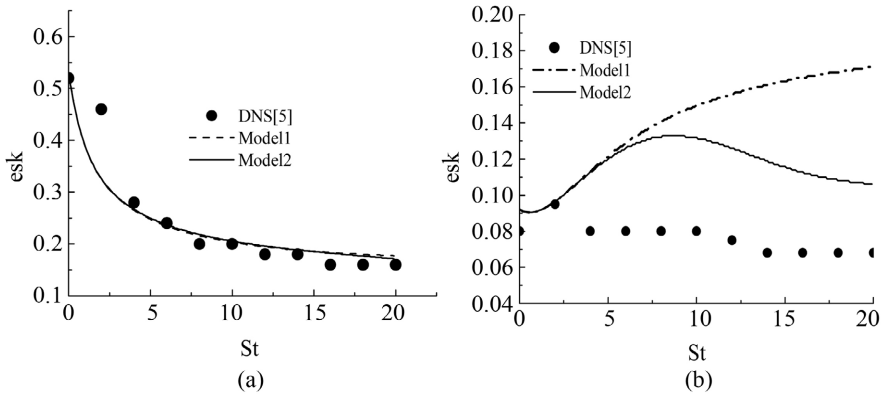

Figure 1. Time evolution of the turbulent dissipation in the case A1.

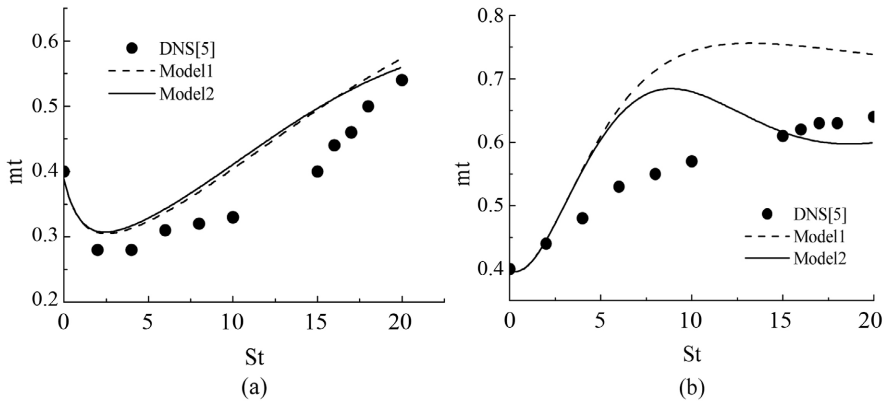

Figure 2. Time evolution of the turbulent Mach number in the cases: (a) A1, (b) A4.

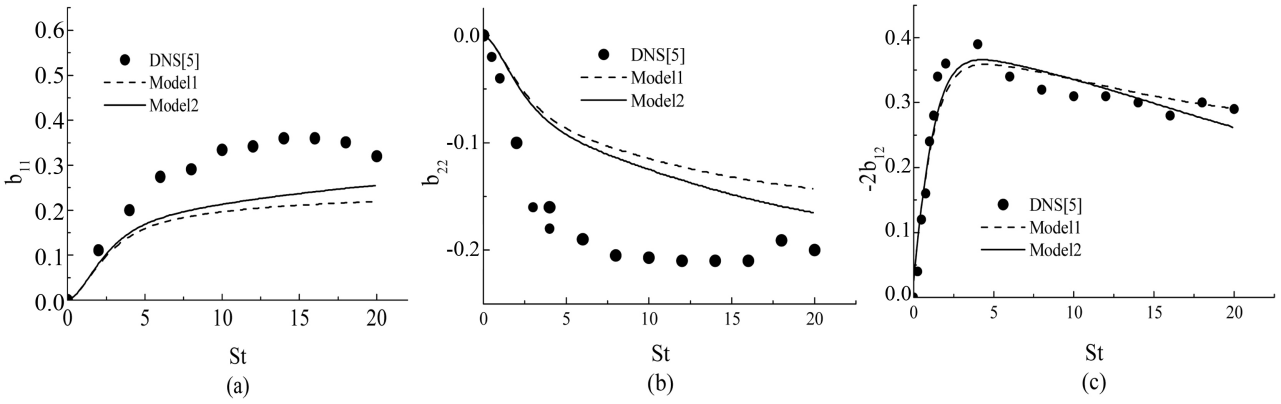

Figure 3. Time evolution of the turbulent Reynolds stress anisotropies in the case A1: (a) b_{11}, (b) b_{22}, (c) b_{12}.

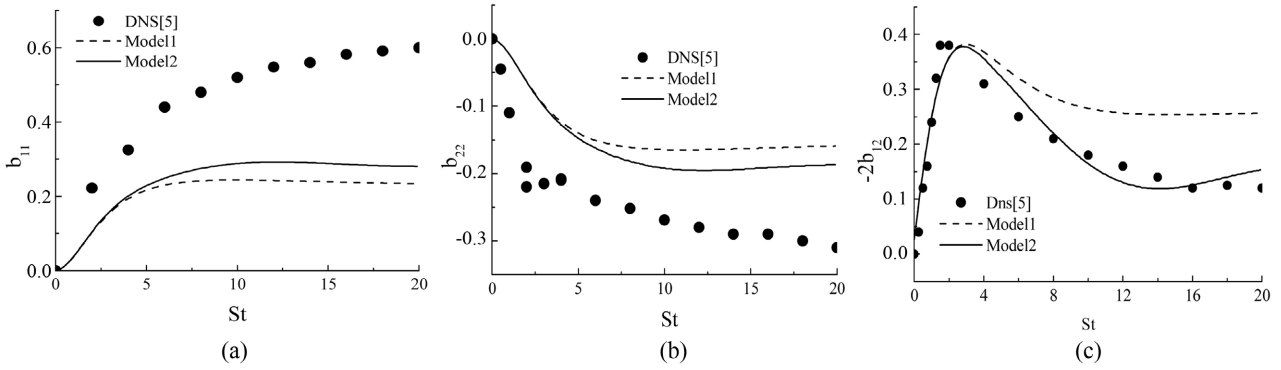

Figure 4. Time evolution of the turbulent Reynolds stress anisotropies in the case A1: (a) b_{11}, (b) b_{22}, (c) b_{12}.

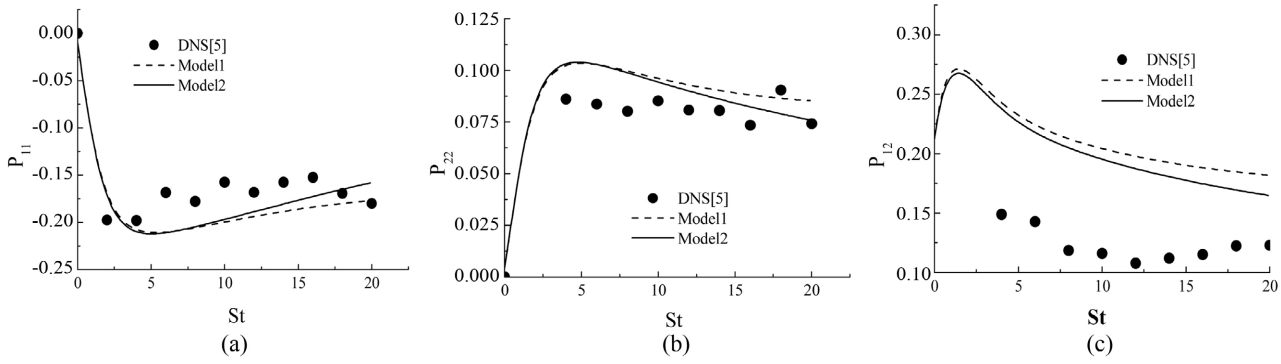

Figure 5. Time evolution of the normalized pressure strain components in the case A1: (a) P_{11}, (b) P_{22}, (c) P_{12}.

All the cases of DNS [5] correspond to different initial conditions listed in Table 2. We consider two DNS [5] cases: A1 and A4 which correspond respectively to low and high compressibility effects. From all figures, one can see an accuracy of model 2 in prediction compressible homogeneous shear flow.

Figure 1(a) and Figure 1(b) present the behavior of the normalized dissipation ε_s/Sk, for cases A_1 and A_4. There is a decrease in ε_s/Sk when M_g increases. In regard, the relation, ($\varepsilon_s/Sk = -2b_{12}\varepsilon_s/P$), between the previous different turbulent quantities, the cause of this discrepancy can be found in the strong reduction of the Reynolds turbulent shear stress b_{12} which is significantly affected by

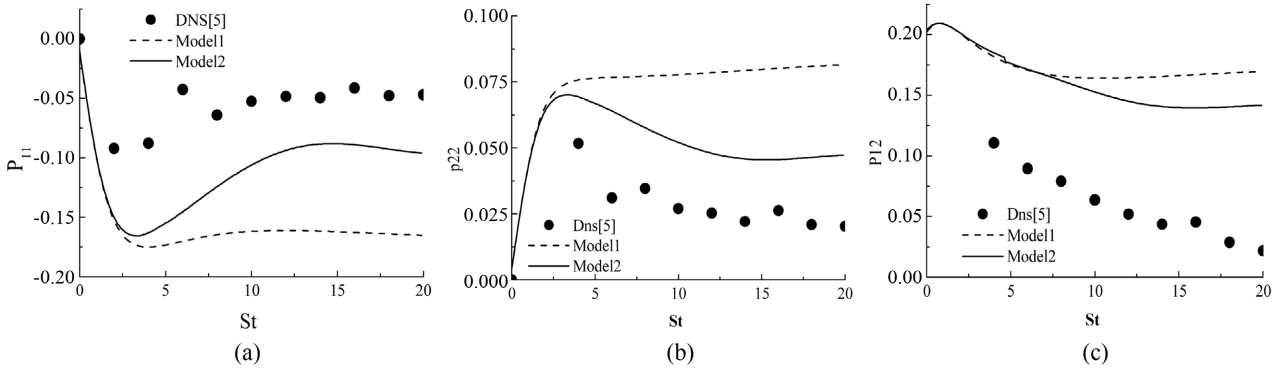

Figure 6. Time evolution of the normalized pressure strain components in the case A4: (a) P_{11}, (b) P_{22}, (c) P_{12}.

Table 2. Initial conditions for compressible homogeneous shear flow: DNS [5].

Case	M_{t0}	$(\varepsilon_s/SK)_0$	M_{g0}	b_{11}	b_{22}	b_{12}
A1	0.4	1.8	0.22	0	0	0
A2	0.4	3.6	0.44	0	0	0
A3	0.4	5.4	0.66	0	0	0
A 4	0.4	10.8	1.32	0	0	0

compressibility effects from numerical simulation cases A_1 to A_4 of the previous DNS results. It is clear that the models 1 and 2 agree the DNS [5] results for the case A1. But in the case A4, the models are different, one can see that the proposal model follows the trend of the increase ε_s/Sk for initial time, ($st \le 5$) and the decreased for later time. However, the predicted values of ε_s/Sk from the model 1 show a systematic increase with the time in disagreement with the DNS for earlier time.

The predicted turbulent Mach number with the models 1 and 2 are plotted in **Figure 2(a)** and **Figure 2(b)**. It is clearly seen that the tow models appear to be able to predict the time increase of the turbulent Mach number for the case A1. The models are nearly similar, the difference between their predictions are smaller. For the case A4, the model 1 over-predict the turbulent Mach number, one can see an unphysical equilibrium values of the turbulent Mach number are predicted with this model. However, the model 2 now yields good equilibrium predictions for the turbulent Mach number as it is shown by these results.

Figure 3 and **Figure 4** show the non-dimensional time St-variation of the Reynolds stress anisotropies b_{11}, b_{22} and b_{12} for cases: A_1 to A_4 from DNS [5]. It is clear that all the model 1 and 2 appear to be insensitive to the increase of the streamwise b_{11} and the transverse b_{22} Reynolds stress anisotropies when the compressibility increases. The models results are in disagreement with the DNS data especially at high M_g in case: A_4. But, one can see there is a little difference between the models, with the proposal compressibility correction, the model 2 leads to slight improvement in the prediction of the diagonal components of the Reynolds stress tensor. This is due to the approach modeling of the model 1 [14].

The results for case A_1 are shown in **Figure 3**, Model 1 and model 2 results are in disagreement with the DNS data for the normal stress anisotropies b_{11} and b_{22}, but satisfy the shear stress component b_{12}. For high compressibility as in case A_4, the DNS data show a strong anisotropy changes in Reynolds stress magnitude. **Figure 4** shows the predicted results for case the models 1 and 2 are still unable to predict correct behavior of the normal Reynolds stress anisotropies. As can be seen in **Figure 3** and **Figure 4**, the proposed model 2 is in good accordance with the DNS results for the shear stress anisotropy, this model predict very similar asymptotic DNS values for this component. From **Figure 3** and **Figure 4**, the model 1 does not correctly reflect compressibility effects on the shear stress anisotropy. This model underestimates these turbulent quantities more significantly in case A_4.

Figure 5 and **Figure 6** present the behavior of the pressure strain correlation $P_{ij} = \varphi_{ij}^{*} / 2SK$ for cases A_1 and A_4 from DNS [5]. Model 2 yields results that are in acceptable qualitative agreement with the DNS data especially at high gradient Mach number. Model 1 seems to be insensitive to the increasing of the gradient Mach number which induces strong changes in magnitude of the pressure strain components. For compressible homogeneous highly sheared, it is argued that the pressure strain correlation is the principal term which determines the strong compressibility changes on the anisotropy levels.

From the previous results, one can see that for case A_1 [5] which corresponds to low compressibility, both models: model 1 and model 2 are nearly similar, they predict correct majority turbulence characteristic parameters of compressible homogeneous shear flow. At high compressibility, model1 ignore the levels the initial values of M_{g0} and do not reflect correctly compressibility effects on the anisotropy levels as in cases A4 [5].

The proposed model 2 predictions are much better than those obtained by the model 1.

4.2. Simulation of Compressible Mixing Layers

The flow is governed by the averaged Navier-Stokes equations associated to those describe the energy, the Reynolds stress and the turbulent dissipation. The simplest of resulting continuity, momentum and energy equation for stationary mixing layers can be written as:

$$\left(\bar{\rho}\tilde{U}_i\right)_{,i} = 0 \tag{23}$$

$$\left(\bar{\rho}\tilde{U}_i\tilde{U}_j\right)_{,i} = -\left(\overline{\rho u_i'' u_j''}\right)_{,j} \tag{24}$$

$$\left(\bar{\rho}C_v\tilde{T}\tilde{U}_j\right)_{,j} = -\left(C_v\overline{\rho u_j'' T''}\right)_{,j} + \varepsilon_s + \varepsilon_c - \overline{p' u_{i,i}'} \tag{25}$$

The Reynolds stress is solutions of the follow equation:

$$\left(\bar{\rho}\tilde{U}_m R_{ij}\right)_{,m} = -\left(R_{im}\tilde{U}_{j,m} + R_{jm}\tilde{U}_{i,m}\right) + \left(\overline{\rho u_i'' u_j'' u_m''}\right)_{,m} + \varphi_{ij}^{*} + 2/3\left(\overline{p' u_{i,i}'} - \varepsilon\right)\delta_{ij} \tag{26}$$

The turbulent solenoidal dissipation rate shall be calculated from the classical

model equation, namely:

$$\left(\bar{\rho}\varepsilon_s \tilde{U}_i\right)_{,i} = \bar{\rho}\left(\varepsilon_s/k\right)\left(C_{\varepsilon 1}R_{im}\tilde{U}_{i,m} - C_{\varepsilon 2}\varepsilon_s\right) - \left(C_{\varepsilon 3}\bar{\rho}\left(\varepsilon_s/k\right)R_{im}\varepsilon_{s,m}\right)_{,i} \quad (27)$$

In the above mentioned transport equations, different terms should be modeled, the gradient diffusion hypothesis is used to represent:

- The turbulent heat flux [19]:

$$\overline{\rho u_i'' T''} = -C_T\left(k/\varepsilon\right)\overline{\rho u_i'' u_m''}\tilde{T}_{,m} \quad (28)$$

- The diffusion term [19]:

$$\overline{\rho u_i'' u_j'' u_m''} = -C_s\left(k/\bar{\rho}\varepsilon\right)\overline{\rho u_i'' u_m''}\left(\overline{\rho u_j'' u_m''}\right)_{,m} \quad (29)$$

Results and Discussion

In this study, computation of two free streams of a fully developed compressible mixing layer (see **Figure 7**) is examined. The flows are characterized typically by the parameters $s = \rho_2/\rho_1$ and $r = U_2/U_1$, are respectively the density and velocity ratios, the experiment conditions of Goebel *et al.* [7] are listed in **Table 3**.

The Equations (23)-(29) are solved using a finite difference scheme. The grid of computational physical domain which is rectangular box defined by the set of point (*x*, *y*) has 6666x41 points. The initial profiles for ε_s, $\bar{\rho}$ and $\tilde{T}$ which are not available in the experiment of Goebel *et al.* [7] are generated as:

- The initial profile of the turbulent dissipation is determined from the turbulent viscosity model.

$$\varepsilon_s = -C_\mu \bar{\rho}\left(K^2/\rho u'' v''\right)\tilde{U}_{,y}, \quad C_\mu = 0.09, \quad (30)$$

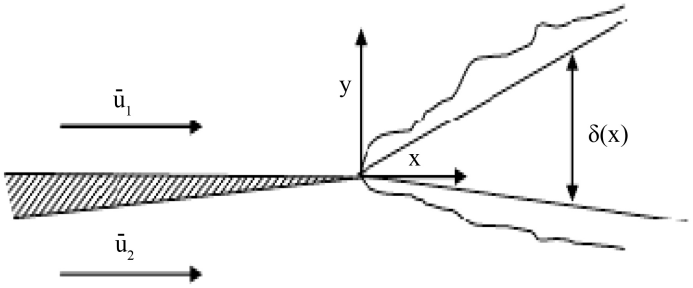

Figure 7. Turbulent mixing layer.

Table 3. Experiment of Goebel and Dutton [7].

M_c	$r = \frac{U_2}{U_1}$	$s = \frac{\rho_2}{\rho_1}$
0.2	0.76	0.78
0.46	0	0
0.69	0	0
0.86	0.16	0.6

- The initial profile of the temperature is obtained from the following similarity:

$$\frac{U-U_2}{U_1-U_2}=\frac{T-T_2}{T_1-T_2}, \tag{31}$$

- The state equation of perfect gas is used to determine the initial profile of the density.

The values of the constants models used in the present simulation are:

$$C_{\varepsilon 1}=1.4,\ C_{\varepsilon 2}=1.8,\ C_{\mu}=0.09,\ C_{\varepsilon}=0.25,\ C_{T}=0.26.$$

According to Sarkar [5], homogeneous shear flow is closely related to the mixing layers, this allows M_g to be connected to M_c. Thus, the coefficients C_i of the Huang *et al.* [12] is expressed as a function of the turbulent Mach number and the convective Mach number as in **Table 4**:

The normalized stream mean velocity $U^*=\left(U-U_2\right)/\left(U_1-U_2\right)$ is represented in relation to the similarity variable $y^*=\left(y-y_c\right)/\delta$ in **Figure 8**, where y is the local cross stream coordinate and y_c is the cross-stream coordinates corresponding to $U^*=0.5$.

The calculated velocity profiles with the models 1 and 2 are in reasonable

Table 4. Numerical coefficients of the pressure strain model.

Model	C_1	C_2	C_3	C_4
Model 1: Huang *et al.* [12]	3.6	0.8	$1.2+0.25\exp\left(-0.05/M_t^3\right)$	$1.2-0.25\exp\left(-0.05/M_t^3\right)$ $1.2+0.25\exp(-0.05/M_t^3)$ $1.2+0.25\exp(-0.05/M_t^3)$
Model 2: proposal model	$3\left(1.0-0.8M_t^2\right)$	$0.8\left(1+0.45M_t^2\right)\mathrm{e}^{-0.015M_c}$	$1.2+0.25\exp\left(-0.05/M_t^3\right)$	$1.2-0.25\exp\left(-0.05/M_t^3\right)$

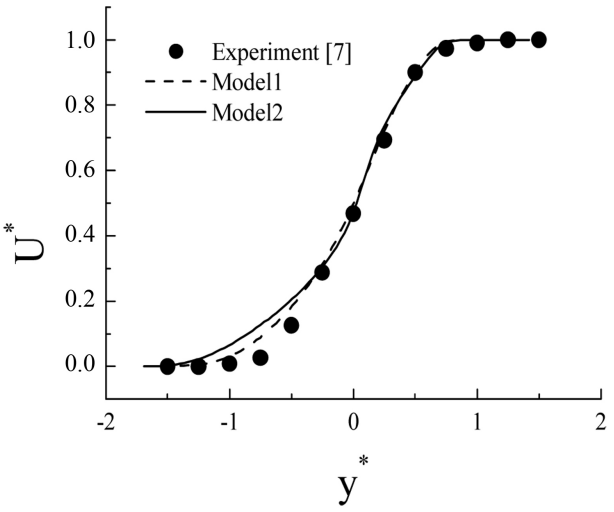

Figure 8. Similarity profiles of the mean velocity U^* for the case: $M_c=0.86$.

agreement with experimental results for the convective Mach number ($M_c = 0.86$).

Figure 9 shows the variation of the turbulent Mach number maximum with the convective Mach number. As can be seen, the model 2 seems to follow the DNS [10] much better than the model 1 for ($M_c = 0.86$).

Figure 10 and Figure 11, present comparison between the Reynolds similarity intensity profiles: the streamwise intensity $R_{11} = \sqrt{\overline{\rho u''^2}} / \overline{\rho}\left(U_1 - U_2\right)^2$, the transverse intensity $R_{22} = \sqrt{\overline{\rho v''^2}} / \overline{\rho}\left(U_1 - U_2\right)^2$, and the shear stress $R_{12} = \overline{\rho u'' v''} / \overline{\rho}\left(U_1 - U_2\right)^2$ obtained from the proposed and [12] models and with experiment results of Goebel and Dutton [7]. It is clear that all the models lead to similar results which are in good accordance with experiment results [7] for small value of convective Mach number ($M_c = 0.2$). When the compressibility effects are more significant ($M_c = 0.86$), it is found that the computed results of the proposed model are in good agreement with the experimental data [7] than those offered

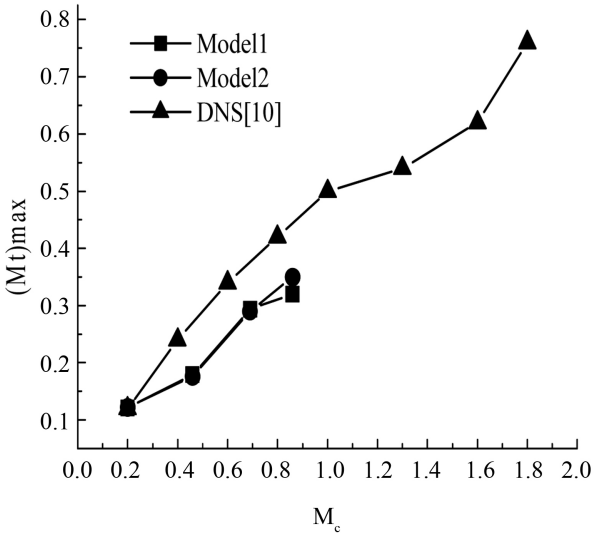

Figure 9. Variation of the maximum turbulent Mach number with the convective Mach number.

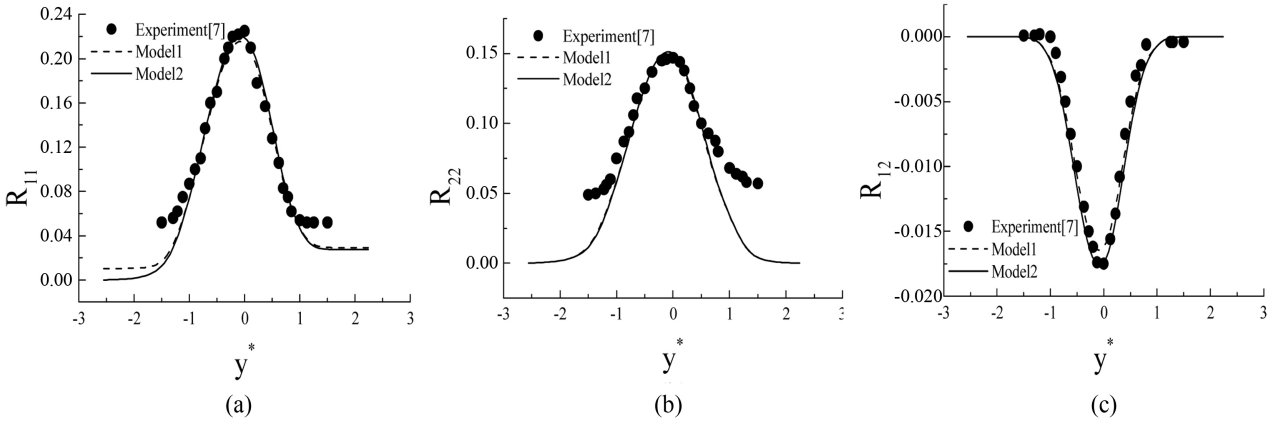

Figure 10. Similarity profiles of the Reynolds intensity: in the cases $M_c = 0.2$: (a): R_{11}, (b): R_{22}, (c): R_{12}.

by the model [12]. From the above results, it is clearly seen that the models 1 and 2 are similar for low convective Mach number. But at high compressibility (the convective Mach number is higher), there is a substantial differences between these models in their predictions. To find the cause of this discrepancy, several studies pointed out on the mechanisms that lead to the dramatic changes of the Reynolds stresses when compressibility increases. It is found that the most important term in the Reynolds stress transport equations is the pressure strain correlation which governs the level of the structural compressibility effects. The maximum values of diverse compressible pressure strain components normalized by its incompressible counterparts ($M_c = 0.2$) are plotted as a function of the convective Mach number in **Figure 12**. It can be seen that the model1does not reproduce the decrease of these turbulent quantities the reduction of this term with increasing M_c is slightly than in DNS results [6] [11]. However, the pressure strain reduction which is the main responsible for the reduction of production term and of the shear layer growth rate appear to be accurately captured by the proposal model 2. Therefore, the convective Mach number is concluded to be important in addition with the turbulent Mach number for modeling the pressure strain in turbulent mixing layers.

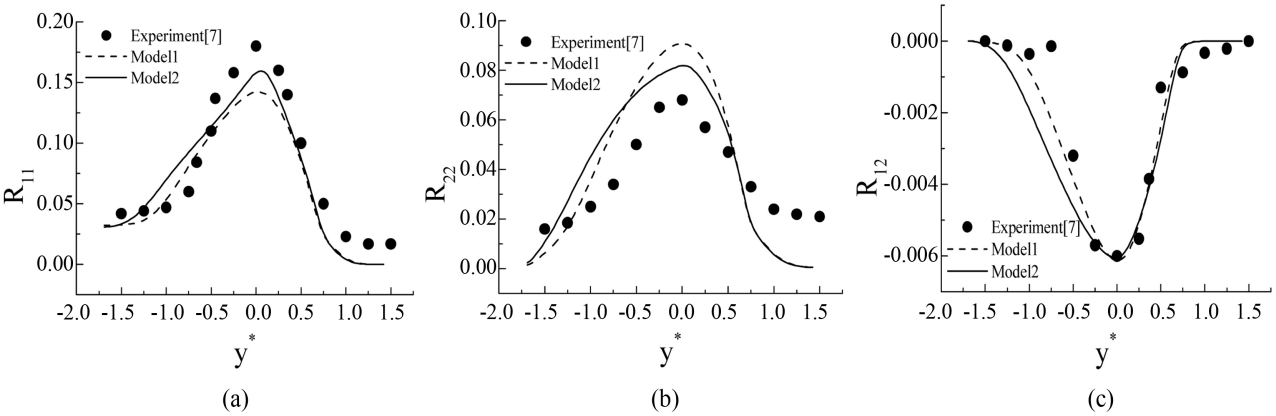

Figure 11. Similarity profiles of the Reynolds intensity: in the cases $M_c = 0.86$: (a): R_{11}, (b): R_{22}, (c): R_{12}.

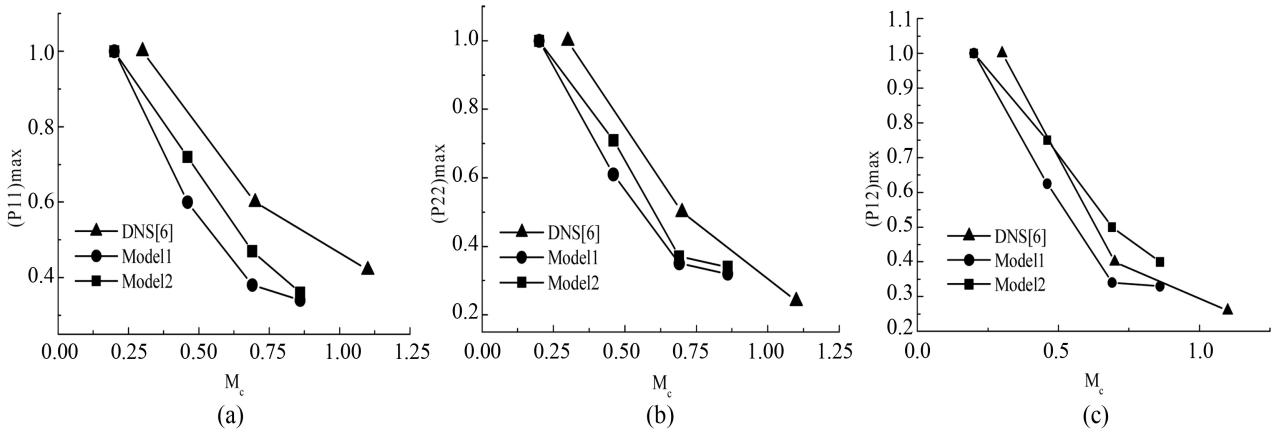

Figure 12. Variation of the maximum pressure strain components with the convective Mach number.

5. Conclusion

In this study, the model of Huang and Fu gives results which do not reflect anisotropy, it gives very poor predictions of the changes in the normal Reynolds-stress anisotropy magnitude but predicts reasonable behavior of shear stress anisotropy and the ratio time scale. A revision of this model of Hung has been proposed to reflect compressibility effects. Application of model 2 to predict compressible homogeneous shear flow shows satisfactory agreement with available DNS [5]. Model 2 appears to be able to predict accurately the structural compressibility effects on homogeneous shear flow as the significant decrease in the magnitude of the Reynolds shear stress and the reduction of the pressures strain components with increasing initial values of the gradient Mach number. Also, model 2 successfully predicts the changes in the compressible mixing layers. Therefore, *a priori*, blending between compressible models is found to be an important issue in the modeling of the pressure-strain correlation.

Conflicts of Interest

The authors declare no conflicts of interest regarding the publication of this paper.

References

[1] Simone, S., Coleman, G.N. and Cambon, C. (1997) The Effect of Compressibility on Turbulent Shear Flow: A Rapid Distorsion-Theory and Direct Numerical Simulation Study. *Journal of Fluid Mechanics*, **330**, 307-338. https://doi.org/10.1017/S0022112096003837

[2] Fujihiro, H. (1999) Effects of Pressure Fluctuations on Turbulence Growth Compressible Homogeneous Shear Flow. *Physics of Fluids*, **A6**, 1625.

[3] Sarkar, S., Erlebacher, G., Hussaini, Y. and Kreiss, H.O. (1991) The Analysis and Modeling of Dilatational Terms in Compressible Turbulence. *Journal of Fluid Mechanics*, **227**, 473-493. https://doi.org/10.1017/S0022112091000204

[4] Blaisdell, G.A. and Sarkar, S. (1993) Investigation of the Pressure-Strain Correlation in Compressible Homogeneous Turbulent Shear Flow. *Transitional and Turbulent Compressible Flows*, **151**, 133-138.

[5] Sarkar, S. (1995) The Stabilizing Effects of Compressibility in Turbulent Shear Flows. *Journal of Fluid Mechanics*, **282**, 163-186. https://doi.org/10.1017/S0022112095000085

[6] Pantano, C. and Sarkar, S. (2002) A Study of Compressibility Effects in the High Speed Turbulent Shear Layer Using Direct Simulation. *Journal of Fluid Mechanics*, **451**, 329-371. https://doi.org/10.1017/S0022112001006978

[7] Goebel, S.G. and Dutton, J.C. (1991) Experimental Study of Compressible Mixing Layers. *AIAA Journal*, **29**, 538-546. https://doi.org/10.2514/3.10617

[8] Samimy, M. and Elliot, G.S. (1990) Effects of Compressibility on the Characteristics of the Free Shear Layers. *AIAA Journal*, **28**, 439-445. https://doi.org/10.2514/3.10412

[9] Vreman, A.W., Sandham, N.D. and Luo, K.H. (1996) Compressible Mixing Layer Growth Rate and Turbulence Characteristics. *Journal of Fluid Mechanics*, **330**, 235-258. https://doi.org/10.1017/S0022112096007525

[10] Freund, J.B., Lele, S.K. and Monin, P. (2000) Compressibility Effects in a Turbulent Annular Mixing Layer. *Journal of Fluid Mechanics*, **421**, 229-267. https://doi.org/10.1017/S0022112000001622

[11] Foysi, H. and Sarkar, S. (2010) The Compressible Mixing Layers: An LES Study. *Theoretical and Computational Fluid Dynamics*, **24**, 565-588. https://doi.org/10.1007/s00162-009-0176-8

[12] Huang, S. and Song, F. (2008) Modelling of Pressure Train Correlation Compressible Turbulent Flow. *Acta Mechanica Sinica*, **24**, 37-43. https://doi.org/10.1007/s10409-007-0127-9

[13] Adumitroaie, V., Ristorcelli, J.R. and Taulbee, D.B. (1999) Progress in Favre Reynolds Stress Closures for Compressible Flows. *Physics of Fluids*, **11**, 2696-2719. https://doi.org/10.1063/1.870130

[14] Park, C.H. and Park, S.O. (2005) Compressible Turbulence Model for the Pressure Strain Correlation. *Journal of Turbulence*, **6**, Article No. N3. https://doi.org/10.1080/14685240500055095

[15] Hamed, M., Hechmi, K. and Taieb, L. (2005) Extension of the Launder Reece and Rodi on Compressible Homogeneous Shear Flow. *The European Physical Journal B*, **45**,147-154. https://doi.org/10.1140/epjb/e2005-00173-8

[16] Hechmi, K. and Taieb, L. (2013) A Compressibility Correction of the Pressure Strain Correlation Model in Turbulent Flow. *Comptes Rendus Mécanique*, **341**, 567-581. https://doi.org/10.1016/j.crme.2013.04.003

[17] Launder, B.E., Reece, G.J. and Rodi, W. (1975) Progress in the Development of a Reynolds-Stress Turbulence Closure. *Journal of Fluid Mechanics*, **68**, 537-566. https://doi.org/10.1017/S0022112075001814

[18] Speziale, C.G., Sarkar, S. and Gatski, T.B. (1990) Modelling the Pressure Strain Correlation of Turbulence an Invariant Dynamical SYSTEMS Approach. *Journal of Fluid Mechanics*, **227**, 245-272. https://doi.org/10.1017/S0022112091000101

[19] Speziale, C.G. and Sarkar, S. (1991) Second Order Closure Models for Supersonic Turbulent Flows. NASA Langley Center, Hampton, ICASE Report 91-9. https://doi.org/10.2514/6.1991-217

Nomenclature

p	Pressure
T	Temperature
t	Time
a	Speed of sound
b_{ij}	Reynolds stress anisotropy
C_p	Specific heat at constant pressure
C_v	Specific heat at constant volume
R	Ideal gas constant
R_{ij}	Reynolds stress
M_t	Turbulent Mach number
M_g	Gradient Mach number
M_c	Convective Mach number
K	Turbulent kinetic energy
u_i	Velocity in the direction xi
d'	Fluctuation of the dilatation
$(.)_{,i}$	Xi-derivative
$(.)_{,t}$	Time-derivative
Greek symbols	
γ	Specific heat ratio
ε	Turbulent dissipation
ε_s	Solenoidal dissipation
ε_c	Compressible dissipation
ρ	Density
μ	Viscosity coefficient
κ	Thermal conductivity coefficient
$\pi_d = \overline{p'd'}$	Pressure-dilatation correlation
P_{ij}^*	Deviator of the pressure strain tensor
δ_{ij}	Kronecker delta
τ_{ij}	Viscous stress tensor
Statistic symbols	
(.)”	Favre fluctuation
(.)’	Reynolds fluctuation
$\tilde{(.)}$	Favre averaged
$\overline{(.)}$	Reynolds averaged